HHS Public Access

Author manuscript

J Bone Miner Res. Author manuscript; available in PMC 2017 August 01.

Published in final edited form as:

J Bone Miner Res. 2016 August ; 31(8): 1608–1616. doi:10.1002/jbmr.2824.

Osteoblast malfunction caused by cell stress response to procollagen misfolding in α2(I)-G610C mouse model of osteogenesis imperfecta

Lynn S. Mirigian[#1,2], **Elena Makareeva**[#1], **Edward L. Mertz**[1], **Shakib Omari**[1], **Anna M. Roberts-Pilgrim**[1], **Arin K. Oestreich**[3], **Charlotte L. Phillips**[4], and **Sergey Leikin**[1]

[1] Section on Physical Biochemistry, Eunice Kennedy Shriver National Institute of Child Health and Human Development (NICHD), National Institutes of Health, Bethesda, MD 20892

[2] Department of Cell Biology, University of Texas Medical Branch, Galveston, TX 77555

[3] Division of Biological Sciences, University of Missouri, Columbia, MO 65211

[4] Department of Biochemistry, University of Missouri, Columbia, MO 65211

[#] These authors contributed equally to this work.

Abstract

Glycine (Gly) substitutions in collagen Gly-X-Y repeats disrupt folding of type I procollagen triple helix and cause severe bone fragility and malformations (osteogenesis imperfecta, aka OI). However, these mutations do not elicit the expected Endoplasmic Reticulum (ER) stress response, in contrast to other protein folding diseases. Thus, it has remained unclear whether cell stress and osteoblast malfunction contribute to the bone pathology caused by Gly substitutions. Here we used a mouse with a Gly610 to cysteine (Cys) substitution in the procollagen α2(I) chain to show that misfolded procollagen accumulation in the ER leads to an unusual form of cell stress, which is neither a conventional unfolded protein response stress nor ER overload. Despite pronounced ER dilation, there is no upregulation of BIP expected in the former and no activation of NFκB signaling expected in the latter. Altered expression of ER chaperones αB crystalline and HSP47, phosphorylation of EIF2α, activation of autophagy, upregulation of general stress response protein CHOP, and osteoblast malfunction reveal some other adaptive response to the ER disruption. We show how this response alters differentiation and function of osteoblasts in culture and *in vivo*. We demonstrate that bone matrix deposition by cultured osteoblasts is rescued by activation of misfolded procollagen autophagy, suggesting a new therapeutic strategy for OI.

Keywords

osteogenesis imperfecta; procollagen; osteoblast; autophagy; cell stress

Address correspondence to: Sergey Leikin, National Institutes of Health, Bldg. 9, Rm. 1E-127, Bethesda, MD 20892; phone: 301-594-8314; leikins@mail.nih.gov.

Supporting Information is included in the submission for online publication.

Disclosures

All authors state that they have no conflicts of interest.

Introduction

Bone is a dynamic organ maintained by multiple cell types. Osteoblasts deposit and mineralize bone matrix, osteoclasts demineralize and resorb the matrix, and osteocytes detect mechanical stresses and damage in the matrix where they are embedded. Activity of these cells is regulated by communication with other cells and organs, involving auto-, para- and endocrine signals as well as the parasympathetic nervous system. Bone pathology may result from any disruption in these processes, but the underlying cause is often osteoblast malfunction. Inadequate ability of osteoblasts to differentiate, produce mineralized bone matrix, or properly respond to signals leads to osteoporosis, skeletal dysplasias, and other disorders. [1]

An active osteoblast produces massive amounts of type I collagen, which is the most abundant organic molecule in bone. Collagen fibers form the bone matrix scaffold and provide a template for mineralization, balancing bone hardness and elasticity. Synthesis of procollagen (precursor of collagen) is a major challenge for the cell due to the unique requirements for its folding [2]. Briefly, after translocation into the Endoplasmic Reticulum (ER) lumen, C-terminal regions of two pro-α1(I) and one pro-α2(I) chains of type I procollagen co-assemble into the C-propeptide. Collagen domains of the chains then wind together into a ~300nm-long triple helix, propagating like a zipper towards the N-terminus. N-propeptide folding completes the process. A variety of distinct posttranslational modifications and helper molecules are needed for procollagen folding, export from the ER, trafficking through the cell, secretion, propeptide cleavage, and assembly into fibers [3,4].

Mutations that disrupt type I procollagen folding are responsible for most cases of severe osteogenesis imperfecta (OI), a hereditary disorder characterized by bone malformations and fractures [5]. The most common mutations are substitutions of Gly in the repeating Gly-X-Y sequence of the triple helix, which prevent hydrogen bonding between collagen chains and sterically hinder helix formation. However, the relationship between the folding disruption by Gly-substitutions and the resulting bone pathology in OI is poorly understood. Hypotheses vary from osteoblast malfunction caused by misfolded procollagen in the cell to matrix malfunction caused by secreted mutant molecules, with no consensus on the mechanisms of OI pathophysiology [2,3,5-8]. Typically, protein misfolding in the ER causes ER stress that involves unfolded protein response (UPR) signaling activated by sequestering of binding immunoglobulin protein (BIP) on misfolded chains [9]. Gly-substitutions in the procollagen triple helix do not seem to cause BIP sequestering [10]. It is unclear how they cause osteoblast malfunction and how this malfunction affects bone formation and homeostasis.

Here, we address the latter questions in a G610C mouse with a Gly610 to Cys substitution in the triple helical region of the α2(I) chain, which models a large group of OI patients with the same mutation [11]. These mice have mild to moderately severe OI in heterozygotes (Het) and perinatal lethal OI in homozygotes (Hom). Previous studies of adult Het animals revealed reduced bone matrix deposition [11] that was reversed by sclerostin [12] and TGFβ [13] neutralizing antibodies as well as by an activating mutation in *Lrp5* [12]. We examine how the mutation causes pathology by using Het and Hom cultured cells, embryos,

and neonates. Our findings suggest that accumulation of misfolded procollagen in G610C osteoblasts causes a distinct cell stress response inconsistent with conventional UPR. The osteoblasts do not die but they malfunction, resulting in abnormal bone matrix deposition and mineralization. The misfolded molecules are cleared from the cell through autophagy, activation of which restores the cell function.

Materials and Methods

Lists of reagents (Supplemental Table S1), cell culture media and buffers (Supplemental Table S2), and antibodies/gene expression assays/primers (Supplemental Table S3) are provided in the Supporting Information. All standard assays were performed according to manufacturer's instructions.

Animals

Het G610C mice (B6.129(FVB)-Col1a2^{tm1Mcbr}/J) were purchased from Jackson Laboratories (stock # 007248) and maintained on the C57BL/6J background. Animal care and experiments were performed in accordance with a protocol approved by the NICHD ACUC. Skeletal staining was performed as described in the 2010 Woods Hole Mouse Embryology Module manual. RNA was extracted from freshly dissected parietal bones in Trizol. For Western Blots (WB), parietal bones were stored frozen until needed. For electron microscopy, parietal bones were fixed with 2.5 % glutaraldehyde or with 2% formaldehyde/2 % glutaraldehyde for 4 h at room temperature and then overnight at 4 °C. Collagen and glycosaminoglycan content in embryonic skin was measured with Sircol and Blyscan assays (Biocolor, UK), respectively.

Cell culture

All cells were cultured at 37 °C, 5% CO_2, 5% O_2. Parietal osteoblasts (pOBs) were released from parietal bones of 3-8 day old mice by 3 mg/mL collagenase [(14)] and cultured in pOB growth medium. Bone Marrow Stromal Cells (BMSCs) were isolated from femurs of 17 week old mice as described in [(15)] and cultured in BMSC growth medium. Mouse Embryonic Fibroblasts (MEFs) were isolated from E14.5 embryos as described in [(16)] and cultured in MEF growth medium. Ascorbic acid 2-phosphate was added to all media (Supplementary Table S2), since we observed significant, partially irreversible dedifferentiation of pOBs without ascorbic acid. For passage, pOBs and MEFs were released with 3 mg/mL collagenase followed by 0.05% Trypsin-EDTA. Most pOB experiments were performed without passage (passage 0 cells). Passage 1 and 2 pOBs were used only when larger number of cells was required (Fig 2A,C; Fig 3C; Supplemental Fig S2A,B). Passage 3 to 6 cells were used for MEF experiments.

All treatments were preceded with overnight incubation of confluent cells with fresh growth media, after which cells were incubated in fresh nutrient deprivation medium or in fresh growth medium with drugs or cytokines. The cells were lysed with Trizol for RNA analysis or washed with PBS then lysed with WB lysis buffer for WB.

Procollagen folding and retention

Procollagen folding and retention were measured by pulse labeling with Aha followed by a chase with Met as described in [17]. Briefly, chymotrypsin/trypsin resistant (folding) or all (retention) triple helical domains of procollagen were purified from cell lysates+media (folding) or cell lysates (retention) by pepsin treatment and selective salt precipitation. The fraction of Aha-containing chains was determined by conjugation of Aha with DIBO-AlexaFluor 555 and conjugation of Lys/Hyl with Cy5 followed by gel electrophoresis with fluorescence detection [17]. Collagen cleaved with MMP-1 and labeled with AlexaFluor 488 was added to each sample before the purification, to measure absolute procollagen concentrations as well as to correct for variations in purification yield and Cy5 labeling intensity [18].

BMSC Differentiation

Freshly isolated BMSCs were plated at 20,000 nucleated cells/10cm^2 for CFU-F and CFU-ALP and at 100,000 nucleated cells/10 cm^2 for CFU-OB in sextuplicate. On day 14, the cells were stained with Alkaline Phosphatase Kit (APK) for CFU-ALP (colonies with 15+ APK-positive cells) and then re-stained with Crystal Violet for CFU-F (20+ cell colonies). For CFU-OB (50+ cell colonies with mineralized matrix), the cells were cultured from day 14 to day 28 in an osteogenic medium with regular media changes, fixed and stained with Alizarin Red.

Western blotting

Cell lysates in the WB buffer were denatured at 95 °C for 10 min, followed by electrophoresis and transfer onto nitrocellulose membrane. The membrane was blocked with 5% BSA, incubated with primary antibodies at 4 °C overnight, and labeled with secondary antibodies conjugated to AlexaFluor 488, 555 or 647. Fluorescence intensities of the bands were normalized to β-actin or GAPDH.

RNA analysis

RNA was purified with Direct-zol kit and reverse transcribed with SuperScript III, using random hexamers as primers. Relative mRNA concentrations were measured in triplicate in a 7500 Fast Real Time PCR system (Applied Biosystems) with Taqman gene expression assays based on $\Delta\Delta C_T$ at the same threshold value for all samples. Transcripts from genes expressed by all cells (*Hspa5*, *Cryab*, *Ddit3*, *Cdkn1a*, and *Axin2*) were normalized to *Hprt1* and *B2m* as endogenous controls. *Runx2* and *Sp7* were selected as more appropriate endogenous controls for transcripts from genes expressed predominantly by preosteoblasts, osteoblasts, and osteocytes in pOB cultures and parietal bones (*Col1a1*, *Serpinh1*, *Alpl*, *Bglap*, *Ifitm5*, *Dmp1*, and *Sost*), to avoid artifacts associated with variations in the fraction of other cells in culture and tissues. Transcription of *Runx2* and *Sp7* remained unchanged relative to *Hprt1* and *B2m* during pOB maturation in culture.

For *Xbp1* splicing, 1 μg total RNA was reverse transcribed and amplified in standard PCR. PCR products were analyzed on 2% precast agarose mini gels with ethidum bromide.

Mineralized matrix deposition

12 wells of WT and 12 wells of Het pOBs were plated in growth medium at 2000cells/cm^2. At confluence, 10 nM rapamycin was added to half of the wells. Osteogenic medium was introduced on the next day and changed every 2-3 days. Mineralization in live cultures was assessed by overnight incubation in phenol-red-free osteogenic medium containing 20 μM Xylenol Orange [19] followed by fluorescence detection or by direct detection of mineral autofluorescence. Fixed cultured were stained with Alizarin Red.

Differential Scanning Calorimetry (DSC)

DSC scans were performed as previously described [20]. Briefly, collagen from E18 embryo skin, matrix deposited by cultured pOBs, or cell culture media was purified by pepsin treatment and selective salt fractionation. Thermograms of collagen denaturation were recorded in 2 mM HCl, pH 2.7 or in 0.2 M sodium phosphate, 0.5 M glycerol, pH 7.4, from 10 to 50°C at 0.125 °C/min heating rates in a Nano III DSC instrument (Calorimetry Sciences Corporation). The fraction of molecules containing the mutant chain was determined from DSC thermograms as described in Supplemental Fig. S2.

Raman microspectroscopy

Cells were cultured in growth medium for 3 (pOBs) or 8 (MEFs) weeks with media changes every 2-3 days. The resulting matrix was fixed in 0.7% formaldehyde at room temperature for 4-6 h. Relative ratios of matrix collagen to cell organics were determined from Raman spectra within at least 10 different matrix regions as described in [21].

Electron microscopy

pOBs were cultured in growth medium for 3 weeks on an ACLAR® fluoropolymer film and fixed with 2.5% glutaraldhyde at room temperature for 1 hour. Glutaraldehyde-fixed matrix samples and parietal bones were postfixed in 2% OsO_4, processed into Spurr's epoxy, sectioned, stained with UO_2-acetate and Pb-citrate, and examined in a JEOL 1400 electron microscope at NICHD Imaging core.

Statistical analysis

Average values, standard deviations and standard errors of the mean were calculated from results of separate experiments, assuming normal distribution. Statistical significance (p values) was evaluated from a 2-tailed, heteroscedastic Student's t-test.

Results

Embryonic and neonatal phenotype

In Het-Het breeding pairs, we observed close to the expected 1:2:1 ratio of WT(wild type):Het:Hom embryos at gestational day E18-19, all of which had similar size and appeared to be viable. All Hom neonates died during or within hours of birth, while most Het and WT pups survived to weaning [11]. Examination of dead neonates suggested atelectasis.

Skeletal staining (Fig. 1) of 9 Hom, 15 Het, and 13 WT neonates as well as X-ray radiography (Supplemental Fig. S1) revealed severe bone pathology in Hom and a wide range of pathology in Het mice, covering almost the entire range from Hom to WT. Parietal bones in Hom calvaria were not mineralized (9/9) while frontal bones had reduced mineral (Fig. 1I, Supplemental Fig. S1C). Het mice had similar, but less pronounced mineralization defects (Fig. 1E). All Hom (Fig. 1J) and severely affected (5/15) Het mice had smaller, flared chests with deformed ribs (Fig. 1F). Beads on Hom ribs indicated numerous *in utero* fractures (Supplemental Fig. S1C, inset). WT (Fig. 1B, Supplemental Fig. S1A) and less affected Het (Supplemental Fig. S1B) mice had normal rib cages. All Hom mice had severely deformed scapulas and multiple long bone defects (Fig. 1K,L, Supplemental Fig. S1C). Severely affected Het mice had occasional scapula (3/15) and long bone (2/15) deformities (Fig. 1G), while WT and less affected Het mice had no deformities (Fig. 1B-D). Many Hom (8/9) and Het (6/15), but not WT (2/13) mice had perinatal fractures (Supplemental Fig. S1B,C), which indicated bone fragility and could have resulted from birth, trampling in the cage, or sample preparation.

Procollagen folding and secretion

Disruption of procollagen folding is the first expected pathogenic effect of a Gly-substitution in the triple helix [3]. To detect it, we utilized pulse-chase labeling with azidohomoalanine (Aha), which replaces methionine (Met) in newly synthesized polypeptides [17,22]. Aha does not affect procollagen synthesis or folding and, unlike radioisotopes, does not elicit cell stress response during pulse-chase experiments [17].

In cultured Het primary parietal osteoblasts (pOBs) and mouse embryonic fibroblasts (MEFs), which produce a 50/50 mixture of molecules with and without the mutant α2(I) chain (not distinguished by our assay), 50% folding of all molecules was observed ~5 min later than in WT cells (Fig. 2A,B). In Hom MEFs, which produce only the mutant molecules, 50% folding was delayed by ~10 min (Fig. 2B). This folding delay resulted in overhydroxylation and overglycosylation of procollagen chains, which migrated slower on gel electrophoresis (Fig. 2E,F).

The residence time (50% retention time) of Aha-labeled procollagen in Het pOBs and MEFs was increased by ~30 min and in Hom MEFs by ~60 min (Fig 2C,D). Such large increases were unlikely to be caused by the 5-10 min delay in folding of mutant molecules, indicating that a fraction of procollagen molecules was misfolded and retained inside mutant cells. Yet, procollagen secreted by Het cells was an approximately 50/50 mixture of molecules with and without the mutant α2(I) chain (Supplemental Fig. S2A) similar to the expected composition in the ER at equal expression of the two *Col1a2* alleles. Apparently, Het cells retained molecules with and without the mutant chain.

Intracellular accumulation and degradation of misfolded procollagen

Retention of misfolded molecules resulted in ~1.7 times more procollagen inside Het than WT pOBs (Fig. 3A). We found no additional procollagen accumulation upon inhibiting proteasome by bortezomib or inhibiting export of unfolded chains from the ER for proteosomal degradation by eeyarestatin. Bortezomib slightly decreased procollagen

synthesis in WT pOBs (c.f. Fig. 3B and 3C). As reported earlier [23], MG132 and lactacystin had much stronger off-target effects (Supplemental Fig. S3A,B). They also did not cause additional procollagen accumulation (data not shown).

Misfolded procollagen molecules appeared to be degraded by lysosomes via (macro)autophagy. Inhibition of autophagosome fusion with lysosomes and lysosomal degradation by bafilomycin A1 and chloroquine increased intracellular procollagen amount and residence time in treated Het cells compared to both untreated Het and treated WT cells (Fig. 3B-C). Autophagy enhancement by nutrient deprivation or rapamycin reduced intracellular procollagen in Het pOBs to the level observed in WT cells, but did not affect WT pOBs (Fig. 3B). Note that chloroquine also caused additional procollagen accumulation in WT cells, likely by inhibiting secretion [24]. Similar effect of bafilomycin A1 was much smaller. Other commonly used autophagy (3-methyladenine, aka 3MA) and lysosome (NH_4Cl/leupeptin) inhibitors did not work in our pOB cultures, as they did not result in the accumulation of an autophagy cargo protein, p62 (Supplemental Fig. S3C).

Measurements of LC3-I and LC3-II protein levels confirmed the role of autophagy. LC3 is converted from cytosolic isoform LC3-I into autophagosome-membrane isoform LC3-II, which is rapidly degraded upon autophagosome-lysosome fusion. Het cells had more LC3-I but similar amounts of LC3-II compared to WT cells (Fig. 3D). We hypothesized that increased LC3-I and unchanged LC3-II indicated faster degradation of LC3-II because of faster autophagosome formation and degradation [25]. Indeed, we observed fast accumulation of LC3-II in Het but not in WT osteoblasts within the first 2.5 h after bafilomycin A1 treatment (Fig. 3E). The initial accumulation of LC3-II was caused by inhibition of its degradation, indicating higher autophagy flux. Chloroquine treatment inhibited procollagen secretion before it affected lysosomal degradation, precluding autophagy flux measurement (Supplemental Fig. S3D). Rapamycin or nutrient deprivation treatment caused LC3-I decline due to conversion to LC3-II, which was similar in Het and WT cells, but the resulting increase in LC3-II was between 1.5 to 3 times smaller in Het cells (Fig. 3F, G). Consistent with the increased autophagy flux, Het cells degraded more p62 and LC3-II in response to autophagy activation by rapamycin or nutrient deprivation and therefore accumulated less LC3-II (Fig. 3F,G).

Cell stress response

Electron microscopy of parietal bone osteoblasts in culture and *in vivo* revealed that the accumulation of misfolded procollagen caused ER dilation in Het cells, indicating elevated cell stress (Fig. 4). The ER dilation was more pronounced *in vivo* (Fig. 4A,B) and significantly reduced by rapamycin treatment in culture (Fig. 4F-H). Consistently, we observed strong transcriptional upregulation of a cell stress factor CHOP/*Ddit3 in vivo* and in culture as well as pronounced upregulation of collagen chaperone HSP47/*Serpinh1* and general ER chaperone crystalline αB/*Cryab in vivo* and similar trends in culture (Fig. 5A).

Increased phosphorylation of EIF2α indicated activation of integrated cell stress response in Het cells [26] (Fig. 5B), while unchanged expression of key UPR transducers BIP and spliced *Xbp1* (Fig. 5, Supplemental Fig. S4) were inconsistent with conventional UPR [9]. ER disruption and enhanced autophagy without UPR were previously reported for an alternative

cell stress response pathway termed “ER overload” [27], but we did not see consistent activation of NFκB signaling (Supplemental Fig. S5A,B) expected in ER overload.

Osteoblast malfunction

We did not detect appreciable pOB apoptosis (Supplemental Fig. S6), but we observed significant abnormalities in Het osteoblast differentiation and function. In particular, we measured the total number of colony forming units (CFU) in bone marrow stromal cell (BMSC) cultures from 4 month old mice (CFU-F), the number of colonies positive for alkaline phosphatase (CFU-ALP) and the number of colonies capable of forming mineralized matrix (CFU-OB) in osteogenic media. We observed a general trend of reduced CFU in Het BMSCs, but a large and statistically significant reduction only for CFU-OB, indicating deficient formation of mature osteoblasts (Fig. 6A).

We found a similar differentiation deficiency in pOBs cultured in osteogenic media (Fig. 6B). After 2 weeks in this media, Het pOBs deposited less mineral than WT pOBs (Fig. 6B and Supplemental Fig. S7). Lower transcription of *Bglap* (osteocalcin) and *Dmp1* at day 8 in osteogenic media indicated that the reduced mineral deposition was caused by altered formation of mature Het osteoblasts. Expression of an early osteoblast marker gene, *Alpl* (alkaline phosphatase) was similar in Het and WT cells. Rapamycin treatment partially rescued osteoblast maturation and mineral deposition.

Cultured Het pOBs also had blunted response to exogenous TGFβ1 and WNT3A. We observed no increase in intracellular procollagen and reduced SMAD2 phosphorylation in response to TGFβ1 (Fig. 6E) as well as reduced transcriptional response of the WNT3A target gene *Axin2* (Fig. 6F).

In parietal bones from E18 Het and Hom embryos, we found reduced transcription of mature osteoblast and osteocyte genes *Col1a1*, *Bglap*, *Ifitm5* (BRIL), and *Sost* (sclerostin). In contrast, transcription of *Dmp1*, which is highly expressed in embryonic osteoblasts and postnatal osteocytes [28], was significantly upregulated (Fig. 6C). Postnatal expression of these genes had similar trends in parietal bones from Het animals, but only the changes in *Dmp1* and *Sost* reached statistical significance. Curiously, Het and Hom parietal bones had increased transcription of the TGFβ target gene *Cdkn1a* (Fig. 6D).

Extracellular matrix deposition

To test how malfunction of the cells and secreted mutant molecules outside the cells affected matrix deposition, we measured matrix composition in skin of E18 embryos and in cultures of MEFs and pOBs. E18 Het and Hom skin had reduced collagen weight fraction and increased glycosaminoglycan (GAG) weight fraction (Fig. 7A-C). In the Het skin, only 30% of type I collagen molecules had the mutant chain (Fig. 7D). Cultured Het pOBs and MEFs deposited 2-3 times less collagen/cell than their WT counterparts (Fig. 7E,F), but almost normal collagen deposition was observed in Het pOB culture with rapamycin (Fig. 7F). Like in skin, only 30% of type I collagen molecules in cultured Het matrix had the mutant chain, suggesting that close to half of the secreted molecules with the mutant chain did not incorporate into the matrix (Supplemental Fig. S2). Nevertheless, Hom MEFs that produced only the mutant molecules deposited the same amount of collagen/cell as Het MEFs.

Discussion

Our overall conclusion is that bone pathology in G610C mice is largely related to disruption of osteoblast differentiation and function by accumulation of misfolded procollagen in the cell. The cells survive but malfunction, causing abnormal bone matrix formation, which is at least partially prevented by enhancing misfolded procollagen degradation in the cell by autophagy. Deficient secretion and potential malfunction of mutant collagen in the bone matrix, e.g. formation of aberrant disulfide bonds between type I collagen triple helices observed in Ref. (11), appear to be less important for the pathology. Procollagen autophagy is therefore an appealing target for OI and potentially other disorders caused by procollagen misfolding. These conclusions are based on the following interpretation of our experimental results.

Triple helix folding disruption causes accumulation of misfolded procollagen and unconventional cell stress response

Delayed folding (Fig. 2A,B), slower clearance (Fig. 2C,D), and increased amount of procollagen inside the cell (Fig. 3A) as well as ER dilation (Fig. 4B,D) indicate that the G610C substitution causes significant intracellular accumulation of misfolded molecules. This conclusion is supported by normalization of the procollagen amount inside the cell (Fig. 3B) and ER structure (Fig. 4F) upon enhancement of autophagy that degrades accumulated misfolded molecules.

We hypothesize that the delay in folding of mutant procollagen (Fig. 2A,B) increases the probability of nonproductive association, misfolding and aggregation of procollagen chains [29]. In particular, formation of short triple helices that tie together chains from multiple procollagen trimers might lead to gelatin-like aggregates. Association of normal and mutant molecules into such aggregates might explain why Het cells retain and accumulate misfolded procollagen (Fig. 2C,D, 3A-C) yet secrete an equal number of molecules with and without the mutant chain (Supplemental Fig. S2).

ER dilation (Fig. 4), transcriptional upregulation of *Cryab* (αB crystalline), *Serpinh1* (HSP47), and *Ddit3* (CHOP) (Fig. 5A) and increased phosphorylation of EIF2α (Fig. 5E) provide evidence of elevated cell stress in response to the accumulation of misfolded procollagen. However, the nature of the resulting stress response is not yet clear. Consistent with other Gly-substitutions [10,29], we did not detect activation of key UPR signaling transducers BIP and spliced *Xbp1*, which mediate conventional ER stress response. The increase in EIF2α phosphorylation without BIP upregulation (Fig. 5B) might be caused by PKR, HRI and/or GCN2 kinases within non-UPR forms of integrated cell stress response rather than by the PERK arm of UPR [30], since the latter is mediated by BIP [9].

Our observations also appear to be inconsistent with ER overload response caused by aggregation of some misfolded proteins (e.g. α1-antitrypsin and other serine protease inhibitors) in the ER. The latter is characterized by the lack of conventional UPR, Ca^{2+} release from the ER, activation of NFκB signaling, and degradation of misfolded proteins by autophagy [27]. We detected upregulation of NFκB signaling only in BMSC but not in pOB culture (Supplemental Fig. S5). It is possible, however, that ER overload response does not

activate NFκB signaling in more mature osteoblasts, for which it would be detrimental [31] and that NFκB signaling is not a necessary attribute of the ER overload pathway.

It is tempting to speculate that procollagen triple helix misfolding triggers a distinct type of cell stress response, because the ER machinery involved in the triple helix folding and procollagen export is very different from most other proteins [2-4]. Notably, more pronounced ER dilation (Fig. 4) and transcriptional upregulation of αB crystalline, HSP47, and CHOP (Fig. 5A) indicate much stronger response of G610C osteoblasts *in vivo* than in culture, likely because the cells produce more collagen in their natural environment.

Osteoblast malfunction caused by cell stress response to procollagen misfolding is the primary cause of bone pathology

Our observations suggest that procollagen misfolding causes osteoblast malfunction at multiple levels including deficient differentiation and maturation, abnormal response to TGFβ, WNT and probably other signaling, and deposition of abnormal bone matrix (Fig. 6,7). This malfunction appears to play a key role in bone pathology.

In particular, more severe stress in cells that produce more procollagen explains the failure of Het BMSCs to form mature osteoblasts (Fig. 6A) and inadequate upregulation of osteoblast genes and matrix mineralization by pOBs (Fig. 6B). Deficient osteoblast differentiation and maturation (Fig. 6C) is likely responsible for under-mineralization of rapidly growing bones in Het and Hom neonates (Fig. 1, Supplemental Fig. S2) and more severe bone phenotype in Het neonates compared to adult animals [11]. Moreover, abnormal osteoblast differentiation is a general feature of OI in human patients and animal models [32-34].

The role of the cell stress in osteoblast malfunction might also explain the dichotomy between a blunted osteoblast response to TGFβ (Fig. 6E; Ref. [35]) and beneficial effects of a neutralizing TGFβ antibody for bone [13]. Indeed, an overlap between cell stress and TGFβ signaling pathways, e.g. because both involve Ca^{2+} release from the ER to cytosol [36,37], is potentially responsible for the coexistence of deficient SMAD2 phosphorylation in response to exogenous TGFβ (Fig. 6E) with endogenous over-expression of a TGFβ target gene *Cdkn1a* (Fig. 6D). As a result of the same overlap, the TGFβ antibody may prevent aggravation of the cell stress by TGFβ. The antibody may have other effects as well, because of many different physiological functions of TGFβ.

Comparison of WT, Het and Hom neonates (Fig. 1) further supports the primary role of cell stress and osteoblast malfunction. Mutant molecules comprise 30% of type I collagen in Het matrix (Supplemental Fig. S2) and 100% in Hom matrix, but the total amount of collagen and GAGs deposited in Het and Hom matrix per cell are similar (Fig. 7). Given this similarity and genetic similarity of G610C animals backcrossed onto an inbred C57BL/6J mouse line, it is difficult to explain the extreme severity of Hom neonates and very wide range of bone pathology in Het neonates by malfunction of secreted mutant collagen. Even the amount of collagen deposited by osteoblasts in the matrix appears to be affected more by the cell malfunction than by deficient incorporation of the secreted mutant molecules into the matrix, as suggested by the rescue of collagen deposition with rapamycin (Fig. 7F). The

phenotypic variability of G610C animals is more likely to be related to the inherent dependence of cell stress response and therefore osteoblast malfunction on multiple genetic, epigenetic and environmental factors.

Autophagy of misfolded procollagen is a key adaptive response affecting the severity of osteoblast cell stress and malfunction

In particular, osteoblast malfunction depends on the ability of the cell to reduce the stress by degrading retained misfolded molecules. Our observations and studies of other Gly substitutions indicate that misfolded procollagen is primarily degraded by lysosomes, to which it is delivered by autophagosomes through activation of (macro)autophagy pathway[29,34]. Inhibition of autophagy increases accumulation of misfolded procollagen in G610C osteoblasts (Fig. 3A,B) while enhancement of autophagy prevents such accumulation (Fig. 3A,B), eliminates ER dilation (Fig. 4E-H), and restores normal ability of the cells to produce and deposit collagen matrix (Fig. 7F).

The latter observations suggest a potential strategy for therapeutic intervention in OI by targeting autophagy and other adaptive cell stress responses. On a cautionary note, however, drug and nutrient based autophagy modulation might also affect other cellular processes. We hope that our ongoing study of direct genetic modulation of autophagy will help clarify the extent to which autophagy enhancement might prevent osteoblast malfunction, although such modulation might have its own off-target effects.

Supplementary Material

Refer to Web version on PubMed Central for supplementary material.

Acknowledgements

This work was funded in part by the Intramural Research Program of NICHD. Study design: LSM, EM, ELM, and SL. Data collection, analysis and interpretation: LSM, EM, ELM, SO, AMR, AKO, CLP, and SL. Drafting manuscript: LSM, EM, ELM, SO, CLP, and SL, Approving final version of the manuscript: LSM, EM, ELM, SO, AMR, AKO, CLP, and SL. SL takes responsibility for the integrity of the data analysis. Electron Microscopy was performed at the NICHD Microscopy and Imaging core with the assistance of Dr. Louis (Chip) Dye.

References

1. Rosen, CJ. Primer on the metabolic bone diseases and disorders of mineral metabolism. 8th ed.. Wiley-Blackwell; Ames, Iowa: 2013. p. 1078
2. Makareeva E, Aviles NA, Leikin S. Chaperoning osteogenesis: new protein-folding disease paradigms. Trends Cell Biol. 2011; 21(3):168–76. [PubMed: 21183349]
3. Makareeva, E.; Leikin, S. Collagen Structure, Folding and Function.. In: Shapiro, JR.; Byers, PH.; Glorieux, FH.; Sponseller, PD., editors. Osteogenesis Imperfecta. Elsevier; Amsterdam: 2014. p. 71-84.
4. Ishikawa Y, Bachinger HP. A molecular ensemble in the rER for procollagen maturation. Biochim Biophys Acta. 2013; 1833(11):2479–91. [PubMed: 23602968]
5. Shapiro, JR.; Byers, PH.; Glorieux, FH.; Sponseller, PD. Osteogenesis Imperfecta. Elsevier; Amsterdam: 2014. p. 555
6. Glorieux FH, Moffatt P. Osteogenesis imperfecta, an ever-expanding conundrum. J Bone Miner Res. 2013; 28(7):1519–22. [PubMed: 23696068]

7. Forlino A, Cabral WA, Barnes AM, Marini JC. New perspectives on osteogenesis imperfecta. Nat Rev Endocrinol. 2011; 7(9):540–57. [PubMed: 21670757]
8. Marini JC, Forlino A, Cabral WA, et al. Consortium for osteogenesis imperfecta mutations in the helical domain of type I collagen: regions rich in lethal mutations align with collagen binding sites for integrins and proteoglycans. Hum Mutat. 2007; 28(3):209–21. [PubMed: 17078022]
9. Hetz C. The unfolded protein response: controlling cell fate decisions under ER stress and beyond. Nat Rev Mol Cell Biol. 2012; 13(2):89–102. [PubMed: 22251901]
10. Chessler SD, Byers PH. BiP binds type I procollagen pro alpha chains with mutations in the carboxyl-terminal propeptide synthesized by cells from patients with osteogenesis imperfecta. J Biol Chem. 1993; 268(24):18226–33. [PubMed: 8349698]
11. Daley E, Streeten EA, Sorkin JD, et al. Variable bone fragility associated with an Amish COL1A2 variant and a knock-in mouse model. J Bone Miner Res. 2010; 25(2):247–61. [PubMed: 19594296]
12. Jacobsen CM, Barber LA, Ayturk UM, et al. Targeting the LRP5 pathway improves bone properties in a mouse model of osteogenesis imperfecta. J Bone Miner Res. 2014; 29(10):2297–306. [PubMed: 24677211]
13. Grafe I, Yang T, Alexander S, et al. Excessive transforming growth factor-beta signaling is a common mechanism in osteogenesis imperfecta. Nat Med. 2014; 20(6):670–5. [PubMed: 24793237]
14. Bakker AD, Klein-Nulend J. Osteoblast isolation from murine calvaria and long bones. Methods Mol Biol. 2012; 816:19–29. [PubMed: 22130919]
15. Suire C, Brouard N, Hirschi K, Simmons PJ. Isolation of the stromal-vascular fraction of mouse bone marrow markedly enhances the yield of clonogenic stromal progenitors. Blood. 2012; 119(11):e86–95. [PubMed: 22262767]
16. Garfield AS. Derivation of primary mouse embryonic fibroblast (PMEF) cultures. Methods Mol Biol. 2010; 633:19–27. [PubMed: 20204617]
17. Mirigian LS, Makareeva E, Leikin S. Pulse-chase analysis of procollagen biosynthesis by azidohomoalanine labeling. Connect Tissue Res. 2014; 55(5-6):403–10. [PubMed: 25159826]
18. Makareeva E, Han SJ, Vera JC, et al. Carcinomas Contain a Matrix Metalloproteinase-Resistant Isoform of Type I Collagen Exerting Selective Support to Invasion. Cancer Research. 2010; 70(11):4366–74. [PubMed: 20460529]
19. Wang YH, Liu Y, Maye P, Rowe DW. Examination of mineralized nodule formation in living osteoblastic cultures using fluorescent dyes. Biotechnol Prog. 2006; 22(6):1697–701. [PubMed: 17137320]
20. Makareeva E, Mertz EL, Kuznetsova NV, et al. Structural heterogeneity of type I collagen triple helix and its role in osteogenesis imperfecta. J Biol Chem. 2008; 283(8):4787–98. [PubMed: 18073209]
21. Barnes AM, Cabral WA, Weis M, et al. Absence of FKBP10 in recessive type XI osteogenesis imperfecta leads to diminished collagen cross-linking and reduced collagen deposition in extracellular matrix. Hum Mutat. 2012; 33(11):1589–98. [PubMed: 22718341]
22. Dieterich DC, Hodas JJ, Gouzer G, et al. In situ visualization and dynamics of newly synthesized proteins in rat hippocampal neurons. Nat Neurosci. 2010; 13(7):897–905. [PubMed: 20543841]
23. Fineschi S, Reith W, Guerne PA, Dayer JM, Chizzolini C. Proteasome blockade exerts an antifibrotic activity by coordinately down-regulating type I collagen and tissue inhibitor of metalloproteinase-1 and up-regulating metalloproteinase-1 production in human dermal fibroblasts. FASEB J. 2006; 20(3):562–4. [PubMed: 16410344]
24. Neblock DS, Berg RA. Lysosomotropic agents ammonium chloride and chloroquine inhibit both the synthesis and secretion of procollagen by freshly isolated embryonic chick tendon cells. Biochem Biophys Res Commun. 1982; 105(3):902–8. [PubMed: 7092908]
25. Klionsky DJ, Abeliovich H, Agostinis P, et al. Guidelines for the use and interpretation of assays for monitoring autophagy in higher eukaryotes. Autophagy. 2008; 4(2):151–75. [PubMed: 18188003]
26. Kroemer G, Marino G, Levine B. Autophagy and the integrated stress response. Mol Cell. 2010; 40(2):280–93. [PubMed: 20965422]

27. Ekeowa UI, Gooptu B, Belorgey D, et al. alpha1-Antitrypsin deficiency, chronic obstructive pulmonary disease and the serpinopathies. Clin Sci (Lond). 2009; 116(12):837–50. [PubMed: 19426146]
28. Fen JQ, Zhang J, Dallas SL, et al. Dentin matrix protein 1, a target molecule for Cbfa1 in bone, is a unique bone marker gene. J Bone Miner Res. 2002; 17(10):1822–31. [PubMed: 12369786]
29. Ishida Y, Yamamoto A, Kitamura A, et al. Autophagic elimination of misfolded procollagen aggregates in the endoplasmic reticulum as a means of cell protection. Mol Biol Cell. 2009; 20(11):2744–54. [PubMed: 19357194]
30. Pavitt GD. Less translational control, more memory. Elife. 2013; 2:e00895. [PubMed: 23741622]
31. Chang J, Wang Z, Tang E, et al. Inhibition of osteoblastic bone formation by nuclear factor-kappaB. Nat Med. 2009; 15(6):682–9. [PubMed: 19448637]
32. Fedarko NS, Moerike M, Brenner R, Robey PG, Vetter U. Extracellular matrix formation by osteoblasts from patients with osteogenesis imperfecta. J Bone Miner Res. 1992; 7(8):921–30. [PubMed: 1442206]
33. Fedarko NS, Robey PG, Vetter UK. Extracellular matrix stoichiometry in osteoblasts from patients with osteogenesis imperfecta. J Bone Miner Res. 1995; 10(7):1122–9. [PubMed: 7484289]
34. Gioia R, Panaroni C, Besio R, et al. Impaired osteoblastogenesis in a murine model of dominant osteogenesis imperfecta: a new target for osteogenesis imperfecta pharmacological therapy. Stem Cells. 2012; 30(7):1465–76. [PubMed: 22511244]
35. Morike M, Windsheimer E, Brenner R, et al. Effects of transforming growth factor beta on cells derived from bone and callus of patients with osteogenesis imperfecta. J Orthop Res. 1993; 11(4): 564–72. [PubMed: 8340828]
36. Kaufman RJ. Stress signaling from the lumen of the endoplasmic reticulum: coordination of gene transcriptional and translational controls. Genes Dev. 1999; 13(10):1211–33. [PubMed: 10346810]
37. Nesti LJ, Caterson EJ, Li WJ, et al. TGF-beta1 calcium signaling in osteoblasts. J Cell Biochem. 2007; 101(2):348–59. [PubMed: 17211850]
38. Makareeva E, Cabral WA, Marini JC, Leikin S. Molecular mechanism of alpha 1(I)-osteogenesis Imperfecta/Ehlers-Danlos syndrome - Unfolding of an N-anchor domain at the N-terminal end of the type I collagen triple helix. Journal of Biological Chemistry. 2006; 281(10):6463–70. [PubMed: 16407265]

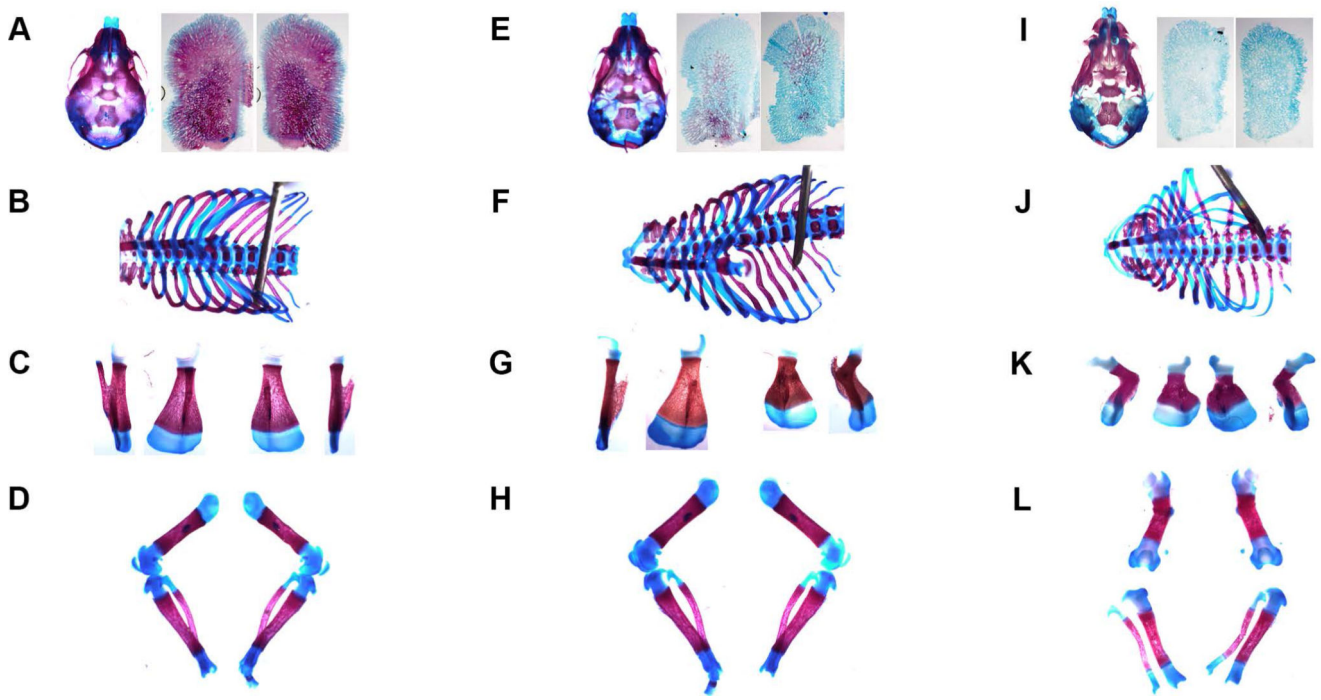

Fig. 1.

Skeletal staining of newborn pups with Alizarin Red (mineral) and Alcian Blue (glycosaminoglycans). (A-D) WT, (E-H) severely affected Het, and (I-L) Hom. (A,E,I) Skulls and enlarged images of separated parietal bones. (B,F,J) Rib cages. (C,G,K) Scapulas; each in two projections, to show deformities. (D,H,L) Femurs, tibias and fibulas; sharp bending of Hom femurs illustrates severe long bone deformities. Separation of hind leg bones was an artifact of sample preparation, resulting from over-digestion of much thinner (vs. WT and Het) ligaments in Hom neonates by KOH during the clearing step of skeletal staining. Each set is from the same mouse. Contrast was digitally enhanced in individual images.

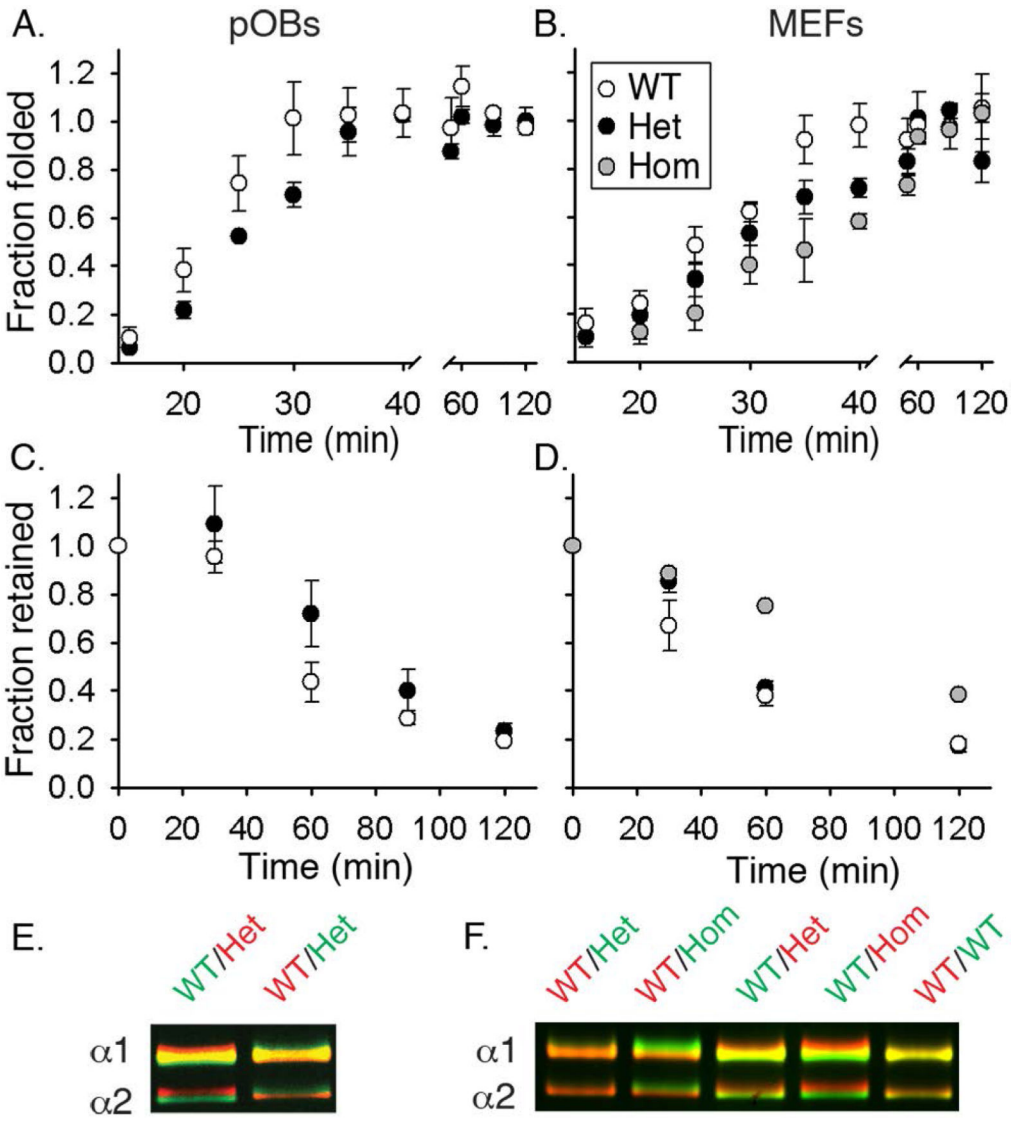

Fig. 2.

Folding, retention and post-translational overmodification of procollagen in cultured pOBs (A,C,E) and MEFs (B,D,F). (A,B) Formation of folded (chymotrypsin/ trypsin resistant), Aha-labeled molecules after a 10 min labeling pulse. 50% folding was observed in ~21 min (WT pOBs), ~ 25 min (Het pOBs), ~ 25 min (WT MEFs), ~ 30 min (Het MEFs), and ~ 35 min (Hom MEFs). (C,D) Fraction of Aha-labeled procollagen remaining inside the cell during a 2 h chase in a Met medium preceded by a 2 h Aha-labeling pulse. 50% retention was observed in ~ 50 min (WT pOBs), ~ 80 min (Het pOBs), ~ 45 min (WT MEFs), ~65 min (Het MEFs), and ~ 100 min (Hom MEFs). (E,F) Procollagen overmodification visualized by delayed electrophoretic migration of the α1(I) and α2(I) chains from triple helical domains purified by pepsin treatment and salt fractionation. Each gel lane contains a binary mixture of molecules from WT cells labeled with either AlexaFluor 488 (green) or Cy5 (red) and molecules from WT, Het or Hom cells labeled with the other dye. Vertical color separation reveals subtle differences in electrophoretic migration of the chains [38]. All

error bars in this and subsequent figures show the standard error of the mean measured in at least triplicate experiments.

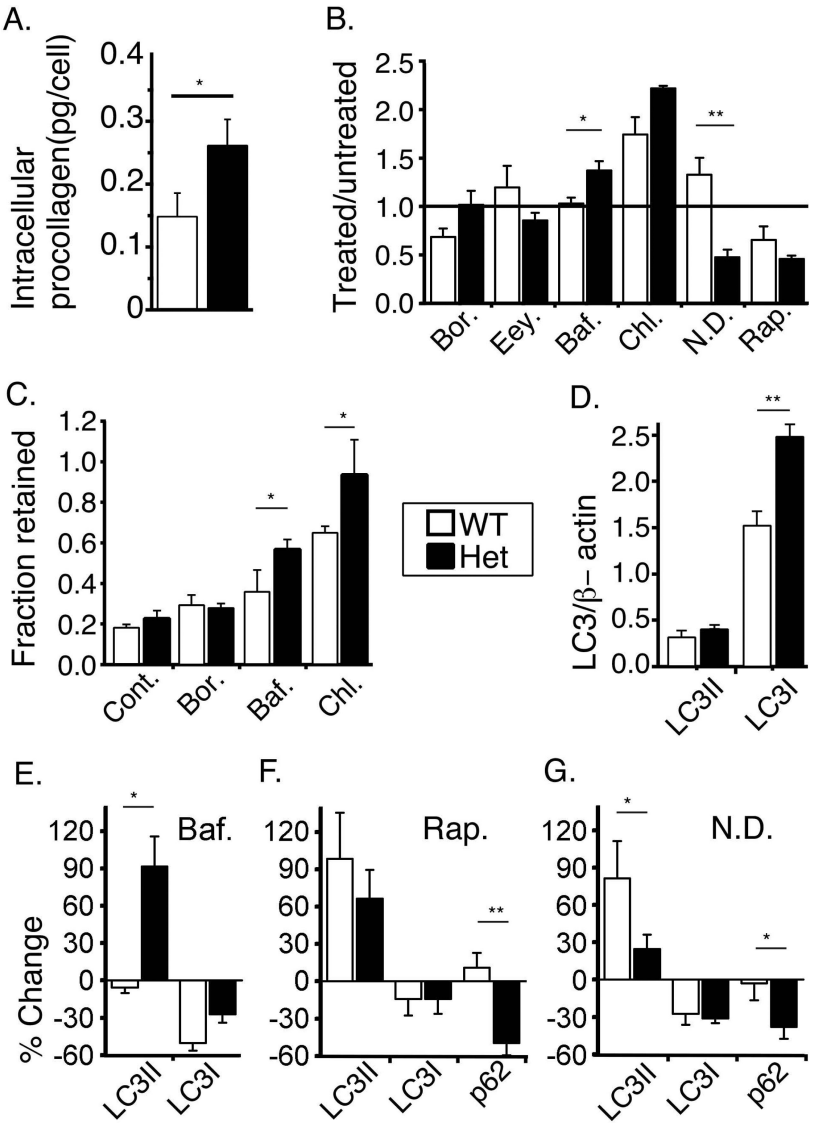

Fig. 3.

Procollagen accumulation and degradation by cultured pOBs. (A) Procollagen amount inside untreated cells. (B) Bortezomib (Bor., 2.6 nM, 6h), eeyarestatin (Eey., 8 μM, 2h), bafilomycin A1 (Baf., 100 nM, 2.5h), chloroquine (Chl., 50 μM, 3h), nutrient deprivation (N.D., 0.5h), and rapamycin (Rap., 10 nM, 1h) effects on procollagen accumulation in the cell measured by western blotting (WB). (C) Bor., Baf., and Chl. effects on the fraction of Aha-labeled procollagen retained in the cell after 2 h Met chase relative to the start of the chase (Cont. – untreated cells). (D) LC3I and LC3II expression relative to β-actin (WB). (E-G) Effects of 2.5h Baf., 1h Rap., and 0.5h N.D. treatment on the expression of LC3II, LC3I and p62 (WB). *, $p<0.05$; **, $p<0.01$.

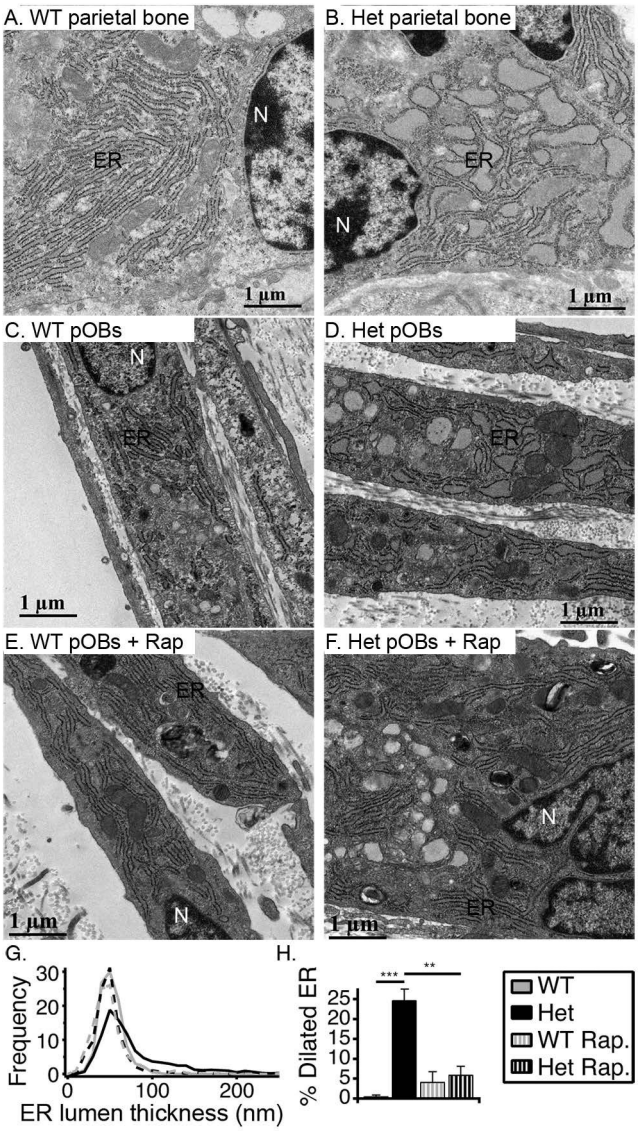

Fig. 4.

Ultrastructural characterization of ER in parietal osteoblasts *in vivo* and in culture by electron microscopy. (A,B). Representative images of osteoblasts in parietal bone from 12 day old WT and Het mice. (C-F). WT and Het pOBs cultured for 3 weeks without and with 10 nM rapamycin (+ Rap). (G). Histograms of ER lumen thickness in cultured pOBs. In culture without Rap, we examined 9 WT and 20 Het cells. In culture with Rap, we examined 14 WT and 11 Het cells. We made 30-180 measurements of ER lumen thickness per cell, depending on the total length of ER cisternae. (H). Fraction of ER length with 100 nm or larger lumen thickness, defined as dilated ER based on the histograms. **, $p<0.01$; ***, $p<0.001$.

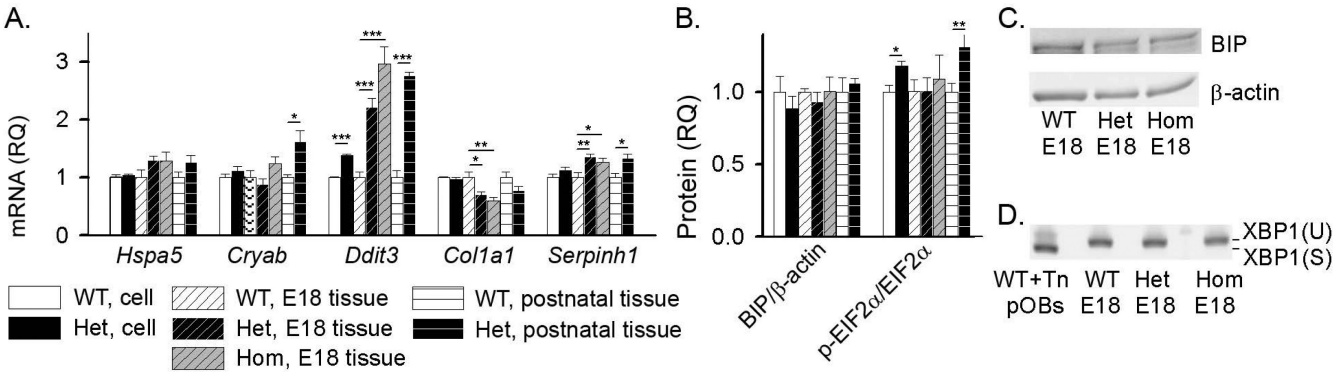

Fig. 5.

Cell stress markers in cultured pOBs and parietal bone from calvaria. (A) Relative quantity (RQ) of *Hspa5* (BIP), *Cryab* (αB crystalline), *Ddit3* (CHOP), *Col1a1*, and *Serpinh1* (HSP47) mRNA with respect to WT in pOB cultures, parietal bones from E18 embryos (7 WT, 9 Het, and 6 Hom), and parietal bones from 17 day old mice (4 WT and 4 Het). (B) BIP protein expression and phosphorylation of EIF2α (measured by WB) in pOBs, parietal bones from E18 embryos (3 WT, 3 Het and 4 Hom) and parietal bones from 2-7 day old mice (6 WT and 6 Het for BIP; 12 WT and 13 Het for p- EIF2α/ EIF2α). (C) Representative WB images for BIP expression in E18 embryos. (D) Analysis of *Xbp1* mRNA splicing (*Xbp1-U* to *Xbp1-S*) by gel electrophoresis after reverse transcription and PCR in parietal bone from E18 embryos. Both *Xbp1-U* and *Xbp1-S* are clearly visible in a positive control of WT pOBs treated for 5 h with 5 μg/mL tunicamycin (Tn), but only *Xbp1-U* was detected in parietal bones from the embryos (as well as in untreated pOB cultures and parietal bones from 2-7 day old mice, Supplemental Fig. S4). *, $p<0.05$; **, $p<0.01$; ***, $p<0.001$.

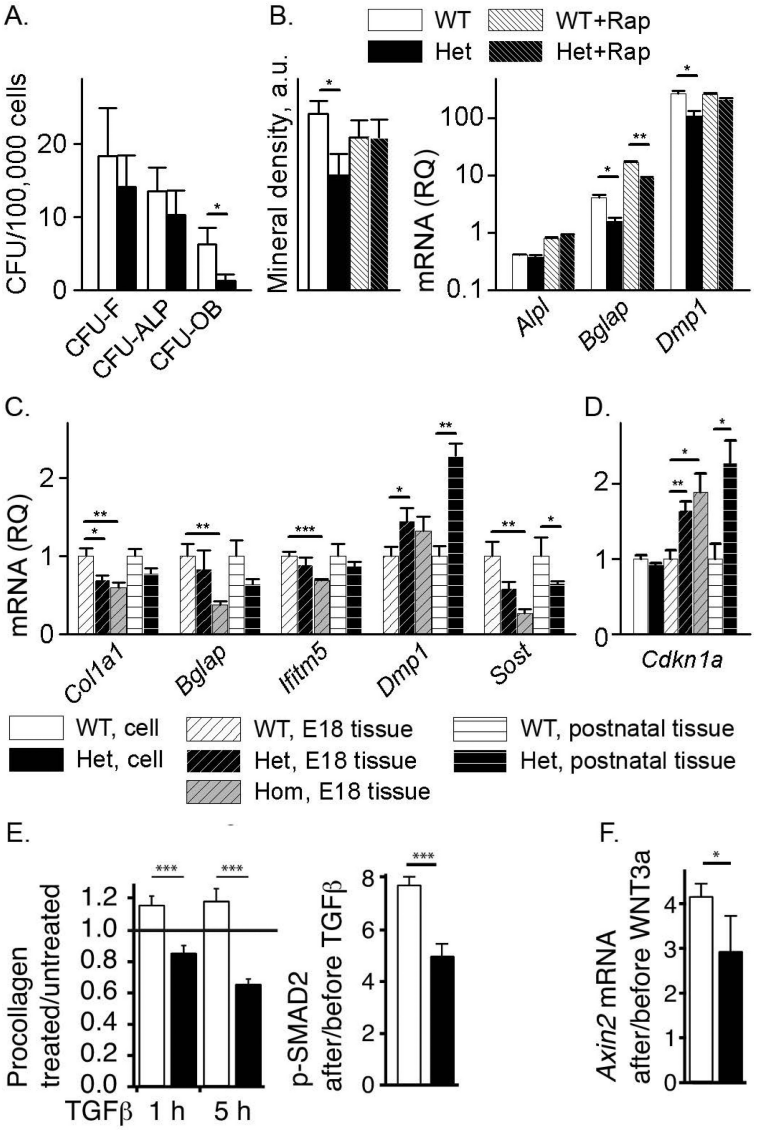

Fig. 6.

Malfunction of Het osteoblasts in culture and parietal bone. (A) Osteoblast differentiation in BMSC culture. (B) Osteoblast maturation in pOB culture without and with 10 nM rapamycin (Rap) assessed by mineral deposition and relative quantity (RQ) of *Alpl* (alkaline phosphatase), *Bglap* (osteocalcin) and *Dmp1* mRNA relative to WT after 8 days in osteogenic media. (C) Relative quantity of *Col1a1*, *Bglap*, *Ifitm5* (BRIL), *Dmp1*, and *Sost* (sclerostin) in parietal bones from E18 embryos (7 WT, 9 Het and 6 Hom) and from 17 day old mice (4 Het and 4 WT). (D) Expression of TGFβ target gene *Cdkn1a* in pOB cultures and parietal bones from the same embryos and animals. (E) Effect of 10 ng/mL TGFβ1 on intracellular procollagen after 1h and 5h and on phosphorylation of TGFβ target SMAD2 after 1h. (F) Effect of 100 ng/mL WNT3A on transcription of WNT target gene *Axin2* after 4 hours. *, $p<0.05$; **, $p<0.01$; ***, $p<0.001$.

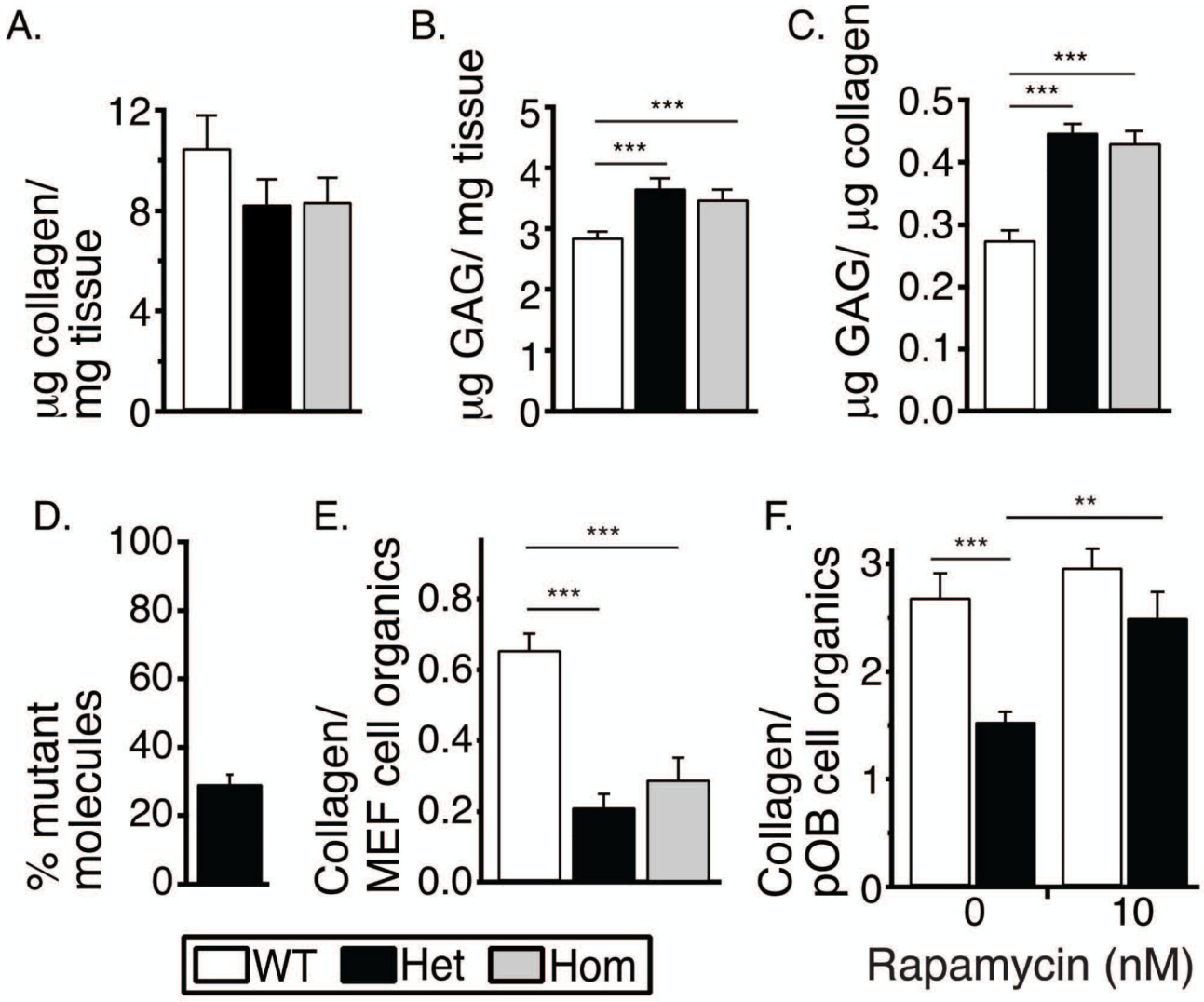

Fig. 7.

Collagen matrix deposition *in vivo* and in culture. (A-C) Collagen and GAG content in skin of WT (n=2), Het (n=3) and Hom (n=2) E18 embryos measured with Sircol and Blyscan assays. (D) Fraction of type I collagen with the mutant chain in E18 Het skin (n=3) measured by differential scanning calorimetry. (E) Collagen deposition per cell in MEFs cultured for 8 weeks measured as a ratio of integral intensities of characteristic spectral peaks detected by Raman microspectroscopy. (F) Collagen deposition per cell in pOB cultured for 3 weeks without and with 10 nM rapamycin measured as in panel E. **, $p<0.01$, ***, $p<0.001$.